



**HAL**  
open science

# Preclinical dosimetry in proton minibeam radiation therapy: Robustness analysis and guidelines

Ramon Ortiz, Ludovic de Marzi, Yolanda Prezado

► **To cite this version:**

Ramon Ortiz, Ludovic de Marzi, Yolanda Prezado. Preclinical dosimetry in proton minibeam radiation therapy: Robustness analysis and guidelines. *Medical Physics*, 2022, 49 (8), pp.5551-5561. 10.1002/mp.15780 . hal-03827276

**HAL Id: hal-03827276**

**<https://hal.science/hal-03827276>**

Submitted on 26 Oct 2022

**HAL** is a multi-disciplinary open access archive for the deposit and dissemination of scientific research documents, whether they are published or not. The documents may come from teaching and research institutions in France or abroad, or from public or private research centers.

L'archive ouverte pluridisciplinaire **HAL**, est destinée au dépôt et à la diffusion de documents scientifiques de niveau recherche, publiés ou non, émanant des établissements d'enseignement et de recherche français ou étrangers, des laboratoires publics ou privés.

# Preclinical dosimetry in proton minibeam radiation therapy: Robustness analysis and guidelines

Ramon Ortiz<sup>1,2</sup> | Ludovic De Marzi<sup>3,4</sup> | Yolanda Prezado<sup>1,2</sup>

<sup>1</sup>Institut Curie, Université PSL, CNRS UMR3347, Inserm U1021, Signalisation Radiobiologie et Cancer, Orsay, France

<sup>2</sup>Université Paris-Saclay, CNRS UMR3347, Inserm U1021, Signalisation Radiobiologie et Cancer, Orsay, France

<sup>3</sup>Centre de Protonthérapie d'Orsay, Radiation Oncology Department, Campus Universitaire, Institut Curie, PSL Research University, Orsay, France

<sup>4</sup>Institut Curie, Campus Universitaire, PSL Research University, University Paris Saclay, INSERM LITO, Orsay, France

## Correspondence

Ramon Ortiz, Institut Curie Centre de Recherche, Campus Universitaire Bâtiment 110, 91405 Orsay, France.  
Email: [ramon.ortiz@curie.fr](mailto:ramon.ortiz@curie.fr)

## Funding information

European Research Council (ERC), Grant/Award Number: 817908; SIRIC, Grant/Award Number: INCa-DGOS-Inserm\_12554; France Life Imaging, Grant/Award Number: ANR-11-INBS-0006

## Abstract

**Purpose:** Proton minibeam radiation therapy (pMBRT) is a new radiotherapy approach that has shown a significant increase in the therapeutic window in glioma-bearing rats compared to conventional proton therapy. The dosimetry of pMBRT is challenging and error prone due to the submillimetric beamlet sizes used. The aim of this study was to perform a robustness analysis on the setup parameters utilized in current preclinical trials and provide guidelines for reproducible dosimetry. The results of this work are intended to guide upcoming implementations of pMBRT worldwide, as well as pave the way for future clinical implementations.

**Methods:** Monte Carlo simulations and experimental data were used to evaluate the impact of variations in setup parameters and uncertainties in collimator specifications on lateral pMBRT dose distributions. The value of each parameter was modified individually to evaluate their effect on dose distributions. Experimental dosimetry was performed by means of high-resolution detectors, that is, radiochromic films, the IBA Razor and the Microdiamond detector. New guidelines were proposed to optimize the experimental setup in pMBRT studies and perform reproducible dosimetry.

**Results:** The sensitivity of dose distributions to uncertainties and variations in setup parameters was quantified. Quantities that define pMBRT lateral profiles (i.e., the peak-to-valley dose ratio [PVDR], peak and valley doses, and peak width) are significantly influenced by small-scale fluctuations in several of those parameters. The setup implemented at the Orsay proton therapy center for pMBRT irradiation was optimized to increase PVDRs and peak symmetry. In addition, we proposed guidelines to perform accurate and reproducible dosimetry in preclinical studies.

**Conclusions:** This study revealed the importance of adopting guidelines and protocols tailored to the distinct dose delivery method and dose distributions in pMBRT. This new methodology leads to reproducible dosimetry, which is imperative in preclinical trials. The results and guidelines presented in this manuscript can ease the initiation of pMBRT investigations in other centers.

## KEYWORDS

dosimetry, Monte Carlo simulations, proton minibeam radiation therapy, spatial fractionation of the dose

## 1 | INTRODUCTION

Proton minibeam radiation therapy (pMBRT) is a novel cancer therapy based on the spatial modulation of the dose.<sup>1</sup> It combines the benefits of submillimetric

spatially fractionated minibeam<sup>2,3</sup> in terms of normal tissue sparing with the more favorable dose conformity of protons, as compared to X-rays. In pMBRT, lateral dose profiles are a succession of high-dose areas, called peaks, followed by areas of low dose, called

This is an open access article under the terms of the [Creative Commons Attribution-NonCommercial-NoDerivs](https://creativecommons.org/licenses/by-nc-nd/4.0/) License, which permits use and distribution in any medium, provided the original work is properly cited, the use is non-commercial and no modifications or adaptations are made.

© 2022 The Authors. *Medical Physics* published by Wiley Periodicals LLC on behalf of American Association of Physicists in Medicine.

valleys.<sup>4</sup> The ratio between peak and valley doses is called the peak-to-valley dose ratio (PVDR), and it is assumed to be a relevant dosimetric parameter for tissue response.<sup>5</sup> These highly heterogeneous dose distributions appear to trigger biological mechanisms that differ from those in conventional seamless radiotherapy techniques. The main potential participants described in the literature include differential vascular effects,<sup>6,7</sup> cell signaling and bystander effects,<sup>8,9</sup> inflammation and immunomodulatory effects,<sup>10,11</sup> and proliferation of stem cells in the valley regions, which may migrate to repair damaged tissue at peak areas.<sup>5,12</sup>

pMBRT has shown a significant reduction in neurotoxicity in both brain<sup>13–15</sup> and skin<sup>16,17</sup> and an equivalent or superior tumor control, as compared to standard proton therapy (PT) in glioma-bearing rats.<sup>18–21</sup> The widening of the therapeutic window provided by pMBRT has raised interest in initiating preclinical investigations at several centers worldwide. Along this line, robust and reproducible dosimetry for preclinical trials is crucial to reliably correlate the physical quantities that characterize pMBRT dose distributions and biological endpoints. The dosimetry of pMBRT is a challenging and error-prone task due to the very small beam sizes used (500–1000  $\mu\text{m}$ ). For those small field sizes, the volume averaging effect and the lack of secondary particle equilibrium start to play a non-negligible role; then, the approximations of classical radiation physics, valid for larger fields (>2 cm diameter), tend to be inaccurate. Therefore, the use of high-spatial-resolution detectors that can resolve highly heterogeneous dose distributions is necessary, for example, radiochromic films, high-resolution diodes or Microdiamond detectors.<sup>4,22,23</sup> Suitable dosimetry protocols for preclinical experiments in minibeam radiation therapy have been proposed elsewhere.<sup>24</sup>

An additional challenge in pMBRT is the increased impact of uncertainties in the setup conditions on the dose distributions, as compared with conventional seamless techniques. The implementation of pMBRT at clinical centers is currently performed by means of multislit collimators<sup>22</sup> attached to the nozzle's exit and combined with both scattered or scanned beams. Some other methods to create minibeam include magnetic focusing<sup>25,26</sup> or scanning dynamic collimators,<sup>27</sup> but they have not yet been implemented in current clinical facilities.

In this study, we performed a robustness analysis on the dosimetry of pMBRT for preclinical experiments by evaluating the impact that different irradiation and geometry parameters may have on dose distributions. Based on the results obtained, we also proposed a series of guidelines for optimizing the experimental setup and performing reproducible dosimetry. In addition, this manuscript presents examples of pMBRT preclinical dosimetry performed by means of experimental measurements and Monte Carlo (MC) calculations.

## 2 | MATERIALS AND METHODS

### 2.1 | Monte Carlo simulations and geometry details

In accordance with the recommendations of AAPM TG-268,<sup>28</sup> the main characteristics of the MC simulations performed in this study are summarized in Table 1, with further specifics provided in the following sections.

### 2.2 | Collimator design

As in previous studies,<sup>22</sup> a divergent collimator, in which the slit tilt follows the beam divergence, was employed to shape the planar minibeam. A 65-mm-thick brass collimator, optimized for proton minibeam generation, was attached to the nozzle exit. Table 2 describes the geometry of the four different collimators used in this study in terms of the number of slits and center-to-center (c-t-c) distances. In all cases, 20 mm  $\times$  400  $\pm$  50  $\mu\text{m}$  slits were considered.

### 2.3 | Experimental dosimetry

Measurements were performed at the pencil beam scanning (PBS) beamline of the Orsay proton therapy center. The proton energy at the isocenter was 100 MeV. For the purpose of this study, lateral dose profiles were measured at several depths in solid water and in water. A 40  $\times$  40  $\times$  40 cm<sup>3</sup> water tank (BluePhantom<sup>2</sup> water tank [IBA, Belgium]) or a stack of 10 20  $\times$  20  $\times$  1 cm solid water slabs (RW3 slab phantom [PTW, Freiburg, Germany]) was employed. Radiochromic films (Gafchromic EBT-XD [Ashland, USA] and Orthochromic OC-1 [OrthoChrome, USA]), as well as the Razor diode (IBA) and PTW-60019 Microdiamond (PTW) detector, were used for the profile measurements. For film measurements, the monitor units employed were adapted to obtain doses within the appropriate range for each film type, particularly by taking care to always have a dose in the valleys higher than 1 and 3 Gy for EBT-XD and OC-1 films, respectively. For measurements with Razor and Microdiamond solid detectors, the detector was moved in the direction of peaks and valleys by 0.1–0.2 mm increments for each data point (minimum step length achievable by the motors of the water tank). Field irradiations were repeated for each data point. As mentioned previously, a homogeneous 5  $\times$  5 cm<sup>2</sup> field was created at the collimator entrance for each irradiation.

Several air gap values between the surface of the phantom and the downstream part of the collimator were utilized, as described in Section 2.4. Unless otherwise stated, the collimator-isocenter distance (CID) was 8.66 cm (maximum nozzle extension).

**TABLE 1** Summary of the main characteristics of Monte Carlo (MC) simulations

Item	Description
Code	TOPAS <sup>29,30</sup> v3.5 (based on Geant4.10.7). Released on June 21, 2020.
Validation	Benchmark and calibration against experimental data from the ICPO beamline <sup>22,31</sup> for PBS and pMBRT irradiations.
Hardware	Simulations were performed on the Joliot Curie-SKL computational cluster. CPUs: 2 × 24-cores Intel Skylake@2.7 GHz (AVX512).
Source description	Monoenergetic 100 MeV proton beams were simulated. Beam characteristics were taken from the parametrization of the PBS beamline, from a 235 MeV cyclotron (IBA, Belgium) of ICPO, described in De Marzi et al. <sup>31</sup> In all cases, a homogeneous 5 × 5 cm <sup>2</sup> field was considered at the collimator entrance. A total of 3.24 × 10 <sup>8</sup> primary histories were lunched per simulation.
Geometry	The PBS beamline of ICPO was modeled as described in De Marzi et al. <sup>31</sup> A mechanical collimator for pMBRT (described in Section 2.2) was also modeled as in Ref. <sup>22</sup> A 40 × 40 × 40 cm <sup>3</sup> water tank or a stack of 10 RW3 solid water slabs were considered to define the irradiated volumes.
Cross-sections	Standard Geant4 physics cross-section data files were used from the physics list built using the Geant4_Modular option with modules recommended for proton therapy ( <i>g4em-standard_opt3</i> , <i>g4h-phy_QGSP_BIC</i> , <i>g4decay</i> , <i>g4ion-binarycascade</i> , <i>g4h-elastic_HP</i> , <i>g4stopping</i> , <i>g4radioactivedecay</i> ).
Transport parameters	The cut for all particles was set to 0.01 mm.
Scored quantities	The <i>DoseToWater</i> discretized volume scorer was used to score absorbed doses. The dose scoring grid was 0.1 mm in the direction of peaks and valleys, 2 mm along the planar minibeam, and 1 mm in depth.
Statistical uncertainties	The global uncertainty, calculated as the average statistical uncertainty of voxels with a dose higher than 50% of the maximum dose, was kept below 1% in all cases.
Post-processing/normalization	The total absorbed dose was normalized to the maximum dose of the profile considered for the sake of comparing experimental and simulated data.

Abbreviations: ICPO, Orsay proton therapy center; PBS, pencil beam scanning; pMBRT, proton minibeam radiation therapy.

## 2.4 | Robustness analysis

We evaluated the effect on dose distributions of possible uncertainties on parameters that define the setup of pMBRT experiments. The parameters considered in this work are:

**TABLE 2** Description of the collimators

Collimator number	Number of slits	c-t-c distance (mm)
1	1	—
2	5	2.8
3	7	2.8
4	5	4.0

Abbreviation: c-t-c, center-to-center.

1. The tilt of the collimator with respect to the beamline ( $\theta$  in Figure 1). The angle between the collimator entrance and the PBS beamline may affect the dose distributions since the divergence of the slits is optimized to always have collinearity with the beam.
2. The translation of the collimator in the two directions perpendicular to the beamline. The translation of the collimator with respect to the center of the beam may affect the homogeneity of the peak heights along the profile.
3. The tilt of the phantom/detector axis with respect to the beamline ( $\alpha$  in Figure 1).
4. The slit width, c-t-c distance between slits, and divergence angles of the slits. The manufacturing process of such micrometric width and divergent multislit collimators may introduce new sources of uncertainty to the collimator specifications, affecting the lateral dose profiles. Such collimators are typically manufactured by means of electrical discharge machining. The slit divergence is defined as the angle of a given slit with respect to the line normal to the collimator surface.
5. The air gap between the collimator exit and the phantom surface. The distance between the phantom and downstream part of the collimator may have an impact on the lateral dose profiles since the quantity of protons scattered by the collimator, which are deposited at valley regions, may increase with the air gap.
6. The CID, which corresponds to snout extension.

Figure 1 shows a schematic representation of these parameters.

We studied, experimentally and by means of MC simulations, how variations in these parameters affect lateral dose profiles. The value of each parameter was modified individually to independently evaluate its effect on dose distributions. Table 3 describes the values studied. Unless otherwise stated, reference values were utilized (see Table 3). A collimator with five slits and a 4 mm c-t-c distance was considered.

For the different configurations, the full width at half maximum (FWHM) of peaks, PVDRs, and peak, valley, and average doses were evaluated.

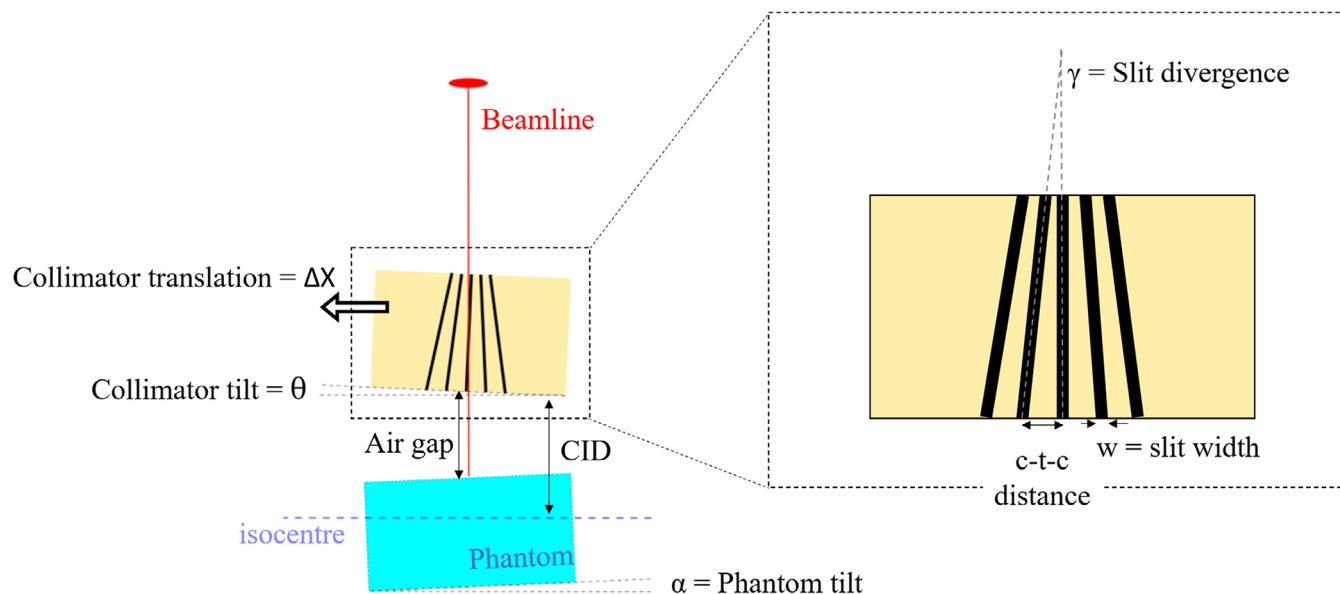


**FIGURE 1** Schematic representation of the parameters studied in the robustness analysis

**TABLE 3** Values considered for the parameters evaluated

Parameter	Values evaluated
Collimator tilt	$0^{\circ a}$ , $\pm 0.125^{\circ}$ , $\pm 0.25^{\circ}$ , and $\pm 0.5^{\circ}$
Collimator translation	$0^a$ and $\pm 2$ mm in $X$ and $Y$ directions
Phantom tilt	$0^{\circ a}$ , $\pm 1^{\circ}$ , and $\pm 3^{\circ}$
c-t-c distance	3.86, 3.93, $4.00^a$ , and 4.15 mm
Slit divergence	$0.100^{\circ}$ , $0.120^{\circ}$ , and $0.125^{\circ a}$
Slit width	350, $400^a$ , and 450 $\mu\text{m}$
Air gap	$5^a$ , 6, and 7 cm
CID	$8.66^a$ and 38.66 cm

Abbreviations: CID, collimator-isocenter distance; c-t-c, center-to-center.

<sup>a</sup>Reference values.

## 2.5 | Optimization of the experimental setup for preclinical experiments

To obtain an optimum setup that allows full exploitation of the benefits of pMBRT, optimization of the beam alignment may be necessary. Indeed, to check and possibly optimize the centering of the beam on the axis of the collimator, 2D profiles were measured with a Lynx detector (IBA), first only using the external rim of the collimator (i.e., seamless conditions) and then using a non-divergent single-slit collimator. This process was repeated for two orientations of the slits, that is, for collimator rotations of  $0^{\circ}$  and  $90^{\circ}$ , until the maximum dose was delivered through the collimator slit, corresponding to the best possible alignment between the collimator and the beamline.

## 3 | RESULTS

### 3.1 | Robustness analysis

For each parameter, the FWHM of peaks, PVDRs, and peak, valley, and mean doses were evaluated in the first 4 cm of the proton range (region of the proton range considered for irradiations in preclinical trials).

#### 3.1.1 | Collimator tilt

The tilt of the collimator with respect to the beamline significantly affects the lateral dose profiles. PVDR decreases by 5%–50% for tilt angles of  $0.125^{\circ}$ – $0.5^{\circ}$ , as compared to the  $0^{\circ}$ -tilt scenario. This is mainly caused by the decrease in peak doses (3%–50%). Valley doses are also affected by the collimator inclination; a maximum variation of -20% was found for tilt angles of  $\pm 0.5^{\circ}$ . Figure 2 illustrates those relative changes with respect to the reference scenario ( $0^{\circ}$ -tilt). Regarding the peak FWHM, an increase up to 50% was found for tilt angles of  $\pm 0.5^{\circ}$ . In addition, the profile is displaced with respect to the center of the phantom, and the average dose decreases significantly (up to 35%). An increasing tilt also reduces the homogeneity of the peak height along the profile. Figure 2 shows an example of lateral dose profiles at a 1 cm depth for the different tilt angles. Similar values were found experimentally (see Section 3.2)

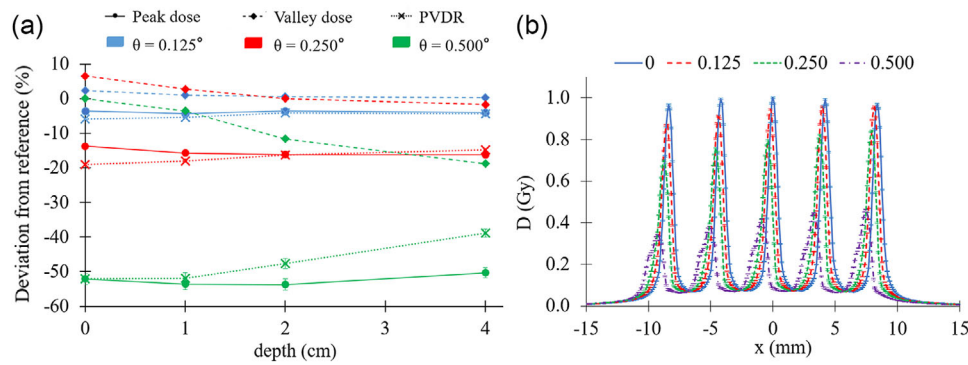


**FIGURE 2** FIGURE 2 (a) Variation in peak-to-valley dose ratios (PVDRs), and peak and valley doses with respect to the reference scenario as a function of the collimator tilt ( $\theta$ ). (b) Lateral dose profiles at a 1 cm depth in water for different collimator tilts with respect to the beamline. The results based on Monte Carlo (MC) simulations

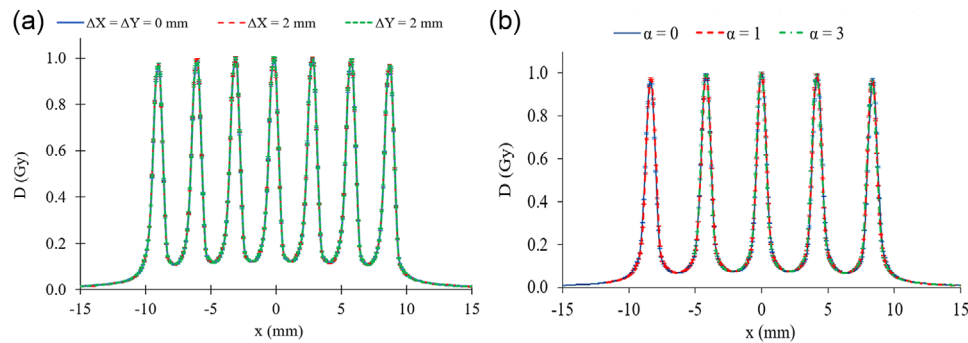


**FIGURE 3** FIGURE 3 Lateral dose profiles at a 1 cm depth in water for (a) different collimator translations with respect to the beamline and (b) different phantom tilt angles with respect to the collimator exit. The results based on Monte Carlo (MC) simulations. Profiles were overlapped for the sake of comparing them

### 3.1.2 | Collimator translation

It was observed that a translation of the collimator with respect to the center of the field in the two directions perpendicular to the beamline does not affect the overall shape of the lateral dose profiles (apart from their position) (see Figure 3).

### 3.1.3 | Phantom tilt

A phantom tilt up to  $\pm 3^\circ$  in the direction of peak and valleys with respect to the downstream part of the collimator does not have an effect on the overall shape of the lateral dose profiles (see Figure 3).

### 3.1.4 | Collimator design: c-t-c distance, slit divergence, and slit width

A variation of the c-t-c distance, the slit divergence or the slit width within the uncertainty from the man-

ufacturing process of the collimator affects the PVDR significantly. A decrease in the c-t-c distance by up to 0.15 mm reduces the PVDR by 5%–6%. This is caused by the increase in the valley doses (up to 7%). In contrast, a 0.15 mm increase in the c-t-c distance leads to an increase in the PVDR and a decrease in valley doses by the same magnitude. Figure 4 illustrates these variations. Peak doses and peak FWHM are not affected by that variation. Conversely, the average dose increases/decreases up to 13% for a 0.15 mm decrease/increase. Decreasing the slit divergence by up to 5% reduces the PVDR by up to 6% since valley doses increase up to 6% (see Figure 4). Consequently, the average dose increases by up to 10%. Peak doses and peak FWHM are not affected by that variation. An increase in the slit width by 50  $\mu\text{m}$  leads to the following effects: a reduction of the PVDR by up to 5%, an increase in the peak and valley doses by up to 19% (see Figure 4), which implies an increment of the average dose by up to 15%, and, finally, an increment of the peak FWHM by 8%. Reverse effects of the same magnitude were found for a 50  $\mu\text{m}$  reduction in the slit width.

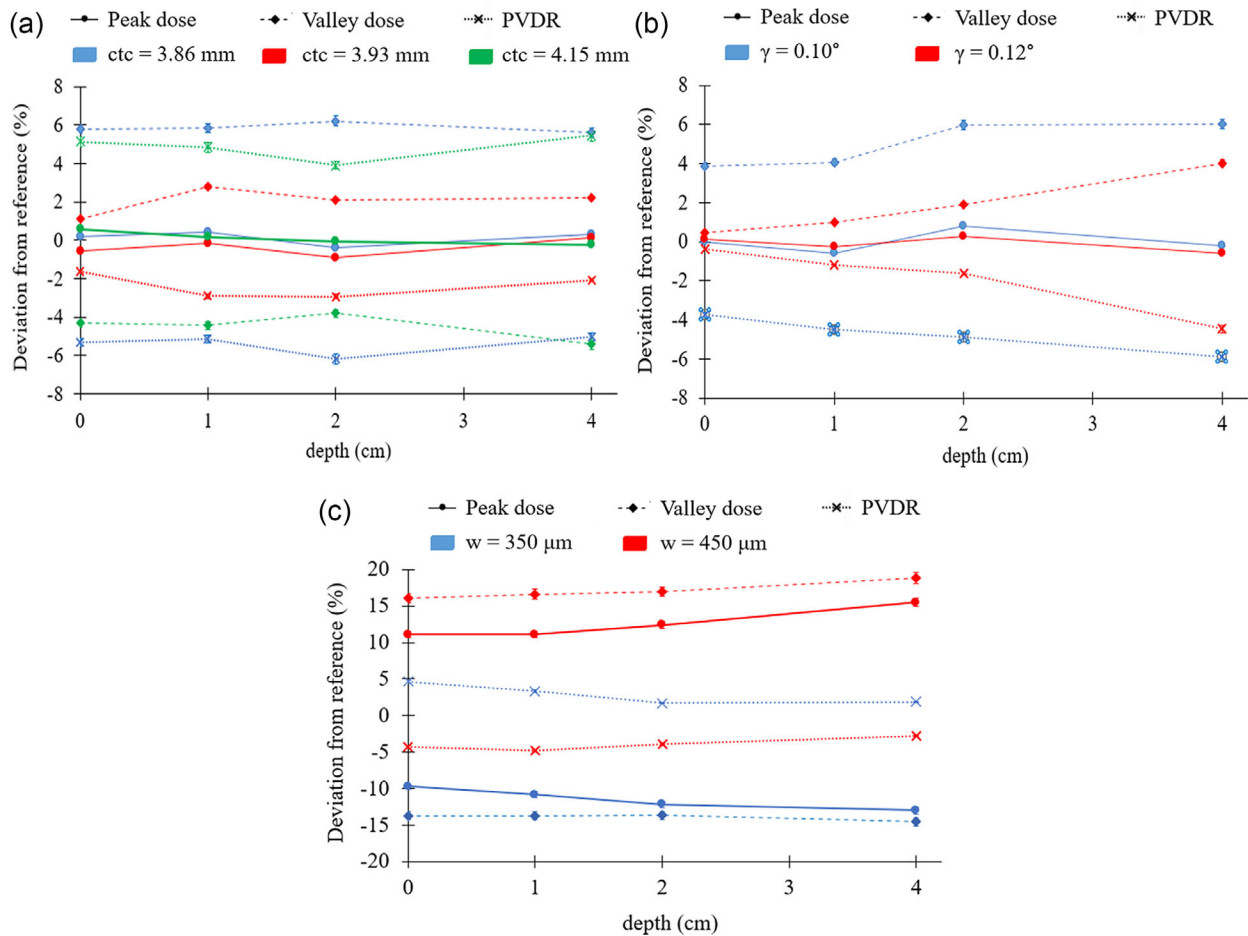


**FIGURE 4** Variation in peak-to-valley dose ratios (PVDRs) and peak and valley doses with respect to the reference scenario as a function of depth and (a) center-to-center (c-t-c) distance, (b) slit divergence ( $\gamma$ ), and (c) slit width ( $w$ )

### 3.1.5 | Air gap

An increment of 1 cm of the air gap between the surface of the phantom and the collimator exit leads to a decrease of up to 14% of the PVDR at shallow depths. Peak doses are reduced by up to 11%, valley doses increase by up to 5% and the average dose is decreased by 4%. These variations decrease as a function of depth, as Figure 5 shows. The peak FWHM increases by 6%–9% for each additional centimeter of air gap.

### 3.1.6 | Collimator-isocenter distance

Experimental and MC results show that snout retraction, that is, an increment of the CID, of 30 cm leads to an increment of peak, valley, and average doses up to 30% and a decrease of 8% of the PVDR.

The impact on dose distributions of the variation in setup parameters is summarized in Table 4.

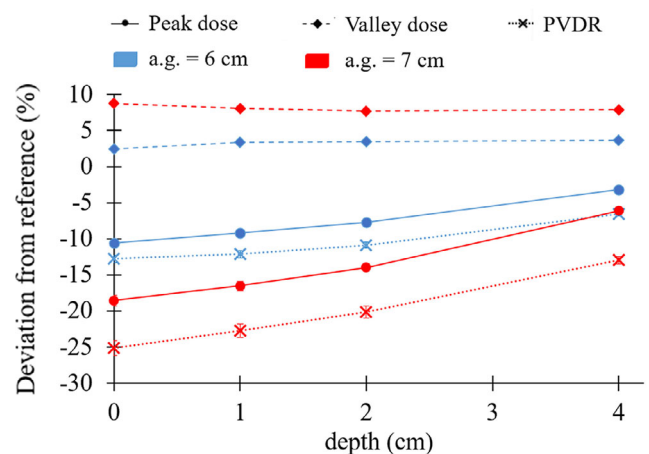


**FIGURE 5** Variation in peak-to-valley dose ratios (PVDRs) and peak and valley doses with respect to the reference scenario as a function of depth and air gap (a.g.)

**TABLE 4** Maximum variation of the peak-to-valley dose ratio (PVDR), full width at half maximum (FWHM), and peak, valley, and average doses for a given variation in the parameters evaluated

Parameter	Variation	Maximum variation (%)				
		PVDR	Peak dose	Valley dose	Average dose	FWHM
Collimator tilt	↗ 0.5°	↘ 50	↘ 50	↘ 20	↘ 35	↗ 50
Collimator translation	↗ 2 mm	0	0	0	0	0
Phantom tilt	↗ 3°	0	0	0	0	0
c-t-c distance	↘ 0.15 mm	↘ 6	0	↗ 7	↗ 13	0
Slit divergence	↘ 5%	↘ 6	0	↗ 6	↗ 10	0
Slit width	↗ 50 μm	↘ 5	↗ 19	↗ 19	↗ 15	↗ 8
Air gap	↗ 1 cm	↘ 14	↘ 11	↗ 5	↘ 4	↗ 9
CID	↗ 30 cm	↘ 8	↗ 30	↗ 30	↗ 30	0

Abbreviations: CID, collimator-isocenter distance; c-t-c, center-to-center.

### 3.2 | Guidelines for robust and reproducible preclinical dosimetry

Given the increased sensitivity of pMBRT dose distributions to setup parameters, as compared to conventional techniques, new guidelines and protocols are needed for reproducible and robust dosimetry in pMBRT preclinical trials. Some examples are proposed below.

#### 3.2.1 | Optimization of the experimental setup

Following the centering of the beam with respect to the collimator, we noticed that the optimization of the collinearity between the beamline and collimator could depend on the orientation and position of the collimator as well as the rotation angle of the gantry. Therefore, an independent optimization, that is, alignment between the beamline and the collimator entrance needs to be done for each irradiation configuration and slit orientation.

Prior to optimization, the tilt angles were  $0.35 \pm 0.05^\circ$ , and using the optimized beam configuration, the tilt was found to be  $0.0 \pm 0.1^\circ$ . Figure 6 illustrates the difference using dose profiles measured with radiochromic films and solid-state detectors. Prior to optimization, the PVDRs were  $5.5 \pm 0.3$  and  $4.8 \pm 0.3$  at depths of 0 and 1 cm, respectively. After beam alignment, the PVDRs increased up to  $9.0 \pm 0.5$  and  $7.5 \pm 0.4$  at depths of 0 and 1 cm, respectively. A higher dose homogeneity between slits, that is, peak doses, by 10% was also observed after the optimization (see Figure 6).

#### 3.2.2 | Dosimetry guidelines

The guidelines proposed for performing reproducible and robust dosimetry in pMBRT preclinical studies are detailed hereafter and summarized in Table 5.

**TABLE 5** Synopsis of the dosimetry guidelines

Objective	Method
Prior to the treatment	
QA of the collimator manufacturing	Experimental measurements and MC/TPS calculations
Selection of the experimental setup	MC/TPS calculations
Absolute dose calibrations	Experimental measurements
During and posttreatment	
QA of the irradiation	Experimental measurements

Abbreviation: QA, quality assurance.

1. Quality assurance (QA) of collimator manufacturing. Measurements with high-resolution detectors (e.g., radiochromic films, Microdiamond or Razor detectors) need to be performed and then compared to results from a benchmarked MC code or treatment planning system (TPS) to characterize the main parameters defining the collimator (i.e., slit width, slit divergence, c-t-c distance).
2. Selection of the experimental setup. Monte carlo or treatment planning system (MC/TPS) simulations using animal CTs may be used for calculating dosimetric quantities of interest, for example, PVDRs. Then, the experimental setup (e.g., a CID and air gap, gantry angle, etc.) that leads to the prescribed dose distributions must be determined. The experimental setup needs to be reproducible, that is, it could be adopted in all phantom and animal irradiations planned for a specific study. This step also implies the selection of the optimum beam configuration for each irradiation configuration and slit orientation.
3. Absolute dose calibration. Absolute dose measurements with high-resolution detectors should be performed at reference positions in a phantom. Figure 7 illustrates examples of these reference measurements using a homogeneous and heterogeneous phantom for preclinical applications, such as for brain or lungs irradiation. Measurements at the ref-

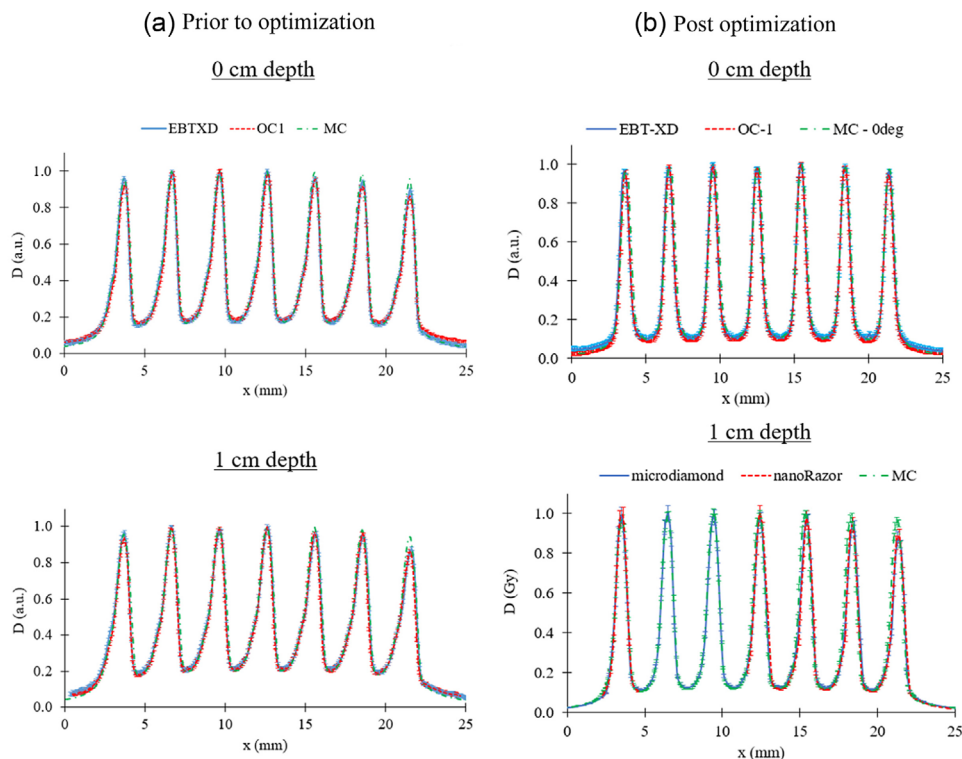


**FIGURE 6** Lateral dose profiles at 0 and 1 cm depths in water (a) before and (b) after the beam alignment optimization. Dose profiles calculated by Monte Carlo (MC) codes and measured with EBT-XD and OC-1 films, and Razor and Microdiamond detectors are presented

erence position should be compared afterwards to MC/TPS predictions. A common practice consists of combining dose measurements at 0 cm depth with calculations at the animal's skin. Those absolute dose measurements are then used for the dose prescription in terms of Monitor Units.

4. QA of the irradiation. At the time of the treatment, radiochromic films should be placed at the rat's skin to measure lateral profiles, which should be compared with the measurements previously performed for dosimetry as a quality check. The measurement of doses at the time of the experiment may also be useful in case irradiations were not reproducible or as prescribed and the dose received by the rat needs to be traced back by means of MC/TPS simulations.

Adopting these guidelines, robust and reproducible dosimetry for preclinical experiments is achieved. Figure 7 illustrates the agreement between dosimetry measurements performed in phantoms prior to the animal's irradiations for the dose prescription and measurements at the animal's skin during the treatment in two different configurations. For instance, for the configuration presented in Figure 7d, the PVDR, peak and valley doses in the reference dosimetry were  $5.6 \pm 0.3$ ,  $70 \pm 3$  Gy, and  $12.4 \pm 0.5$  Gy, respectively, and  $5.9 \pm 0.4$ ,  $68 \pm 3$  Gy, and  $11.8 \pm 0.6$  Gy in the animal irradiation.

Values for the animal irradiation were calculated as an average of different sets of animals treated on different days under the same conditions. Measurements were performed using OC-1 films.

## 4 | DISCUSSION

pMBRT is an innovative radiotherapy technique that uses a strong spatial dose modulation, showing a remarkable increase in the therapeutic index for radioresistant tumors in preclinical experiments.<sup>18–21</sup>

Due to the characteristics of pMBRT (narrow proton beams and lack of lateral equilibrium), the irradiation setup and geometry may have a much higher impact on the pMBRT's highly heterogeneous dose distributions than in conventional techniques. Therefore, a robustness analysis and a best practice guide for dosimetry is highly relevant in pMBRT in order to reliably correlate the biological observations and the dosimetry parameters.

In this study, we evaluated the impact on dose distributions of possible uncertainties on those parameters, that is, variables that define setup and collimator systems, by means of MC simulations and experimental measurements.

We found that slight tilt angles between the beamline and the collimator entrance, not easily detectable in

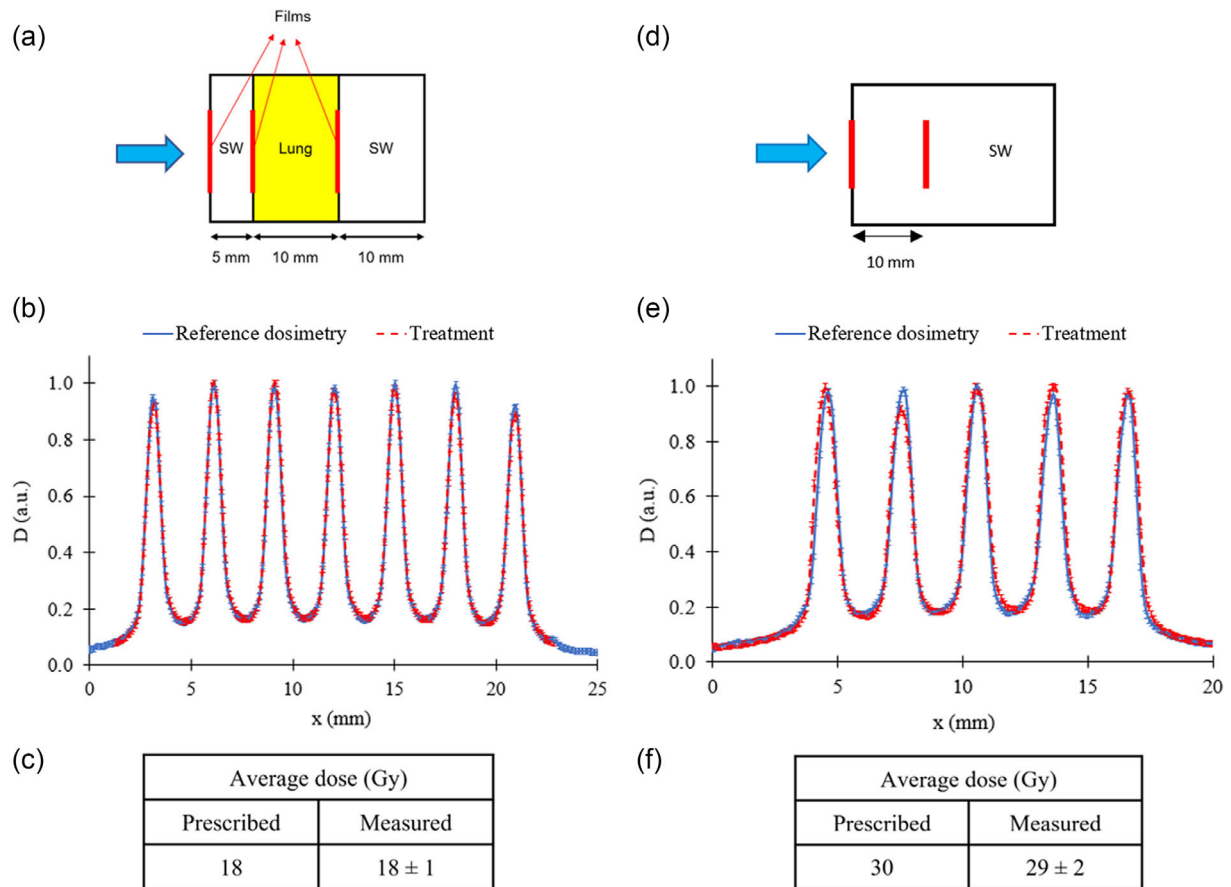


**FIGURE 7** Schematic representation of the experimental setup for the reference dosimetry prior to preclinical lung and brain irradiations (a and d), a comparison of the relative dose profiles measured in the reference dosimetry and small animal irradiation (b and e), and a comparison of the absolute average dose prescribed and measured during the irradiation (c and f). The left and right panels correspond to mouse lung and rat brain irradiations, respectively

clinical QA routines (i.e.,  $\leq 0.5^\circ$ ), significantly impact lateral dose profiles. The PVDR decreases and FWHM increases by up to 50%. This is mainly caused because the divergence of each slit collimator is optimized for the divergence of the PBS beamline, and a tilt leads to a lesser amount of protons passing through each slit, considerably decreasing the peak doses. In contrast, a 5% variation in the slit divergence due to uncertainties in the manufacturing process of the collimator is not large enough to affect peak doses. However, this decrease in the slit divergence angle reduces the PVDR by up to 6% due to the lower distance between minibeam, which increases valley doses since the contribution of scattered protons to this region is greater. For similar reasons, a reduction of the c-t-c distance by the same amount due to uncertainties in the manufacturing process leads to a reduction of the PVDR by 5%–6%. Regarding the slit width, a 50  $\mu\text{m}$  increment in this parameter leads to an increase in peak and valley doses, PVDR, and peak FWHM by up to 19%, 5%, and 8%, respectively, due to the larger proportion of protons passing through the collimator. Such uncertainties are

given by the precision of the system used to manufacture the collimator. A variation in the air gap between the collimator exit and the volume to be irradiated was found to have a significant impact on lateral dose profiles. Each centimeter increment of air gap decreases the PVDR by up to 14% due to the reduction of peak doses and increase of valley doses by up to 11% and 5%, respectively. Peak FWHM also increases by 6%–9%. This is mainly caused by the greater number of scattered protons traveling from peak to valley positions as the air gap increases. Other setup parameters, such as the CID or the translation of the collimator with respect to the beamline axis, may also affect peak and valley doses or displace the profile. Small variations in certain of those parameters are difficult to observe experimentally due to the experimental uncertainty and resolution of the detectors employed; hence, MC simulations are a complementary tool to perform this robustness analysis.

Variations in these geometry and irradiation parameters may influence the biological endpoints of experiments since the dosimetric quantities influenced by

those variations may be highly correlated with the biological responses of normal and tumor tissues. The PVDR is a biologically relevant parameter since it defines the spatial fractionation of the dose: higher PVDR are meant to favor normal tissue sparing.<sup>5</sup> A fluctuation of the peak width (i.e., FWHM) also influences the response of tissues since one of the participants in the normal tissue sparing in pMBRT is the so-called dose–volume effect (the smaller the field size is, the higher the tolerance of normal tissues).<sup>32,33</sup> The increase or reduction of peak and valley doses also plays a crucial role in the normal tissue sparing, especially valley doses since strong indications suggest that these low-dose regions are responsible for the preservation of normal tissue architecture and survival of progenitor cells.<sup>5</sup> In addition, an undesirable variation in the absolute dose may also affect the comparison of pMBRT with conventional broad beam PT since the average dose of lateral profiles is used as the dose prescription parameter in previous and current preclinical trials.<sup>21</sup> A displacement of the profile caused by the variation of some of the parameters studied may also affect the overall response of animals to treatments since normal tissue volumes and tumors may be irradiated or underirradiated, respectively, which is especially relevant in pMBRT due to the high doses employed. Some of these dependencies have also been suggested in other studies.<sup>34</sup> Therefore, the need for a reproducible methodology for robust dosimetry and the precise reporting of irradiation parameters is imperative to extract reliable conclusions from preclinical studies.

## 5 | CONCLUSIONS

This study presents a robustness analysis in the context of pMBRT dosimetry for preclinical trials and provides an insight into the sensitivity of this technique. Unintended variations in setup parameters and uncertainties in the manufacturing process of collimators have an impact on dose distributions, which may bias the correlations between dosimetric quantities and biological endpoints. These findings reveal the need to implement new methodologies to perform robust dosimetry in pMBRT trials. In this work, guidelines for accurate and reproducible dosimetry are proposed and implemented. These results can facilitate the initiation of preclinical investigations in other centers and guide future studies on the clinical implementation of pMBRT.

## ACKNOWLEDGMENTS

This project received funding from the European Research Council (ERC) under the European Union's Horizon 2020 research and innovation program (grant agreement no. 817908), and this project was also partially funded by SIRIC 2018–2022 (INCa-DGOS-Inserm\_12554) and by France Life Imaging, grant

ANR-11-INBS-0006. Calculation time was granted at the supercomputer Joliot Curie SKL (Irene\_skylake) Très grand center de calcul (TGCC) of Commissariat Energie Atomique (CEA), from the Partnership for Advanced Computing in Europe (PRACE Project Access Call 21rst, proposal no. 2020225339).

## CONFLICT OF INTEREST

The authors have no relevant conflicts of interest to disclose.

## REFERENCES

- Prezado Y, Fois GR. Proton-minibeam radiation therapy: a proof of concept. *Med Phys*. 2013;40(3):031712. <https://doi.org/10.1118/1.4791648>
- Dilmanian FA, Zhong Z, Bacarian T, et al. Interlaced X-ray microplanar beams: a radiosurgery approach with clinical potential. *Proc Natl Acad Sci U S A*. 2006;103(25):9709-9714. <https://doi.org/10.1073/pnas.0603567103>
- Prezado Y, Renier M, Bravin A. A new method of creating minibeam patterns for synchrotron radiation therapy: a feasibility study. *J Synchrotron Radiat*. 2009;16(Pt 4):582-586. <https://doi.org/10.1107/S0909049509012503>
- Peucelle C, Nauraye C, Patriarca A, et al. Proton minibeam radiation therapy: experimental dosimetry evaluation. *Med Phys*. 2015;42(12):7108-7113. <https://doi.org/10.1118/1.4935868>
- Dilmanian FA, Button TM, Le Duc G, et al. Response of rat intracranial 9L gliosarcoma to microbeam radiation therapy. *Neuro-Oncol*. 2002;4(1):26-38. <https://doi.org/10.1093/neuonc/4.1.26>
- Sabatasso S, Laissue JA, Hlushchuk R, et al. Microbeam radiation-induced tissue damage depends on the stage of vascular maturation. *Int J Radiat Oncol Biol Phys*. 2011;80(5):1522-1532. <https://doi.org/10.1016/j.ijrobp.2011.03.018>
- Bouchet A, Serduc R, Laissue JA, Djonov V. Effects of microbeam radiation therapy on normal and tumoral blood vessels. *Phys Med*. 2015;31(6):634-641. <https://doi.org/10.1016/j.ejmp.2015.04.014>
- Dilmanian FA, Qu Y, Feinendegen LE, et al. Tissue-sparing effect of X-ray microplanar beams particularly in the CNS: is a bystander effect involved?. *Exp Hematol*. 2007;35(4 suppl 1):69-77. <https://doi.org/10.1016/j.exphem.2007.01.014>
- Asur RS, Sharma S, Chang CW, et al. Spatially fractionated radiation induces cytotoxicity and changes in gene expression in bystander and radiation adjacent murine carcinoma cells. *Radiat Res*. 2012;177(6):751-765. <https://doi.org/10.1667/rr2780.1>
- Bouchet A, Sakakini N, Atifi ME, et al. Early gene expression analysis in 9L orthotopic tumor-bearing rats identifies immune modulation in molecular response to synchrotron microbeam radiation therapy. *PLoS ONE*. 2013;8(12):e81874. <https://doi.org/10.1371/journal.pone.0081874>
- Potez M, Fernandez-Palomo C, Bouchet A, et al. Synchrotron microbeam radiation therapy as a new approach for the treatment of radioresistant melanoma: potential underlying mechanisms. *Int J Radiat Oncol Biol Phys*. 2019;105(5):1126-1136. <https://doi.org/10.1016/j.ijrobp.2019.08.027>
- Fukunaga H, Kaminaga K, Sato T, et al. High-precision microbeam radiotherapy reveals testicular tissue-sparing effects for male fertility preservation. *Sci Rep*. 2019;9(1):12618. <https://doi.org/10.1038/s41598-019-48772-3>
- Lamirault C, Doyère V, Juchaux M, et al. Short and long-term evaluation of the impact of proton minibeam radiation therapy on motor, emotional and cognitive functions. *Sci Rep*. 2020;10(1):13511. <https://doi.org/10.1038/s41598-020-70371-w>
- Prezado Y, Deman P, Varlet P, et al. Tolerance to dose escalation in minibeam radiation therapy applied to normal rat brain: long-

- term clinical, radiological and histopathological analysis. *Radiat Res.* 2015;184(3):314-321. <https://doi.org/10.1667/RR14018.1>
15. Prezado Y, Jouvion G, Hardy D, et al. Proton minibeam radiation therapy spares normal rat brain: long-term clinical, radiological and histopathological analysis. *Sci Rep.* 2017;7(1):14403. <https://doi.org/10.1038/s41598-017-14786-y>
  16. Zlobinskaya O, Girst S, Greubel C, et al. Reduced side effects by proton microchannel radiotherapy: study in a human skin model. *Radiat Environ Biophys.* 2013;52(1):123-133. <https://doi.org/10.1007/s00411-012-0450-9>
  17. Girst S, Greubel C, Reindl J, et al. Proton minibeam radiation therapy reduces side effects in an in vivo mouse ear model. *Int J Radiat Oncol Biol Phys.* 2016;95(1):234-241. <https://doi.org/10.1016/j.ijrobp.2015.10.020>
  18. Prezado Y, Jouvion G, Patriarca A, et al. Proton minibeam radiation therapy widens the therapeutic index for high-grade gliomas. *Sci Rep.* 2018;8:16479. <https://doi.org/10.1038/s41598-018-34796-8>
  19. Prezado Y, Jouvion G, Guardiola C, et al. Tumor control in RG2 glioma-bearing rats: a comparison between proton minibeam therapy and standard proton therapy. *Int J Radiat Oncol Biol Phys.* 2019;104(2):266-271. <https://doi.org/10.1016/j.ijrobp.2019.01.080>
  20. Lamirault C, Brisebard E, Patriarca A, et al. Spatially modulated proton minibeam results in the same increase of lifespan as a uniform target dose coverage in F98-glioma-bearing rats. *Radiat Res.* 2020;194(6):715-723. <https://doi.org/10.1667/RADE-19-00013.1>
  21. Bertho A, Ortiz R, Juchaux M, et al. First evaluation of temporal and spatial fractionation in proton minibeam radiation therapy of glioma-bearing rats. *Cancers.* 2021;13(19):4865. <https://doi.org/10.3390/cancers13194865>
  22. De Marzi L, Patriarca A, Nauraye C, et al. Implementation of planar proton minibeam radiation therapy using a pencil beam scanning system: a proof of concept study. *Med Phys.* 2018;45(11):5305-5316. <https://doi.org/10.1002/mp.13209>
  23. Guardiola C, De Marzi L, Prezado Y. Verification of a Monte Carlo dose calculation engine in proton minibeam radiotherapy in a passive scattering beamline for preclinical trials. *Br J Radiol.* 2020;93(1107):20190578. <https://doi.org/10.1259/bjr.20190578>
  24. Prezado Y, Martinez-Rovira I, Thengumpallil S, Deman P. Dosimetry protocol for the preclinical trials in white-beam minibeam radiation therapy. *Med Phys.* 2011;38(9):5012-5020. <https://doi.org/10.1118/1.3608908>
  25. Schneider T, De Marzi L, Patriarca A, Prezado Y. Advancing proton minibeam radiation therapy: magnetically focussed proton minibeam at a clinical centre. *Sci Rep.* 2020;10(1):1384. <https://doi.org/10.1038/s41598-020-58052-0>
  26. Schneider T, Patriarca A, Degiovanni A, Gallas M, Prezado Y. Conceptual design of a novel nozzle combined with a clinical proton Linac for magnetically focussed minibeam. *Cancers.* 2021;13(18):4657. <https://doi.org/10.3390/cancers13184657>
  27. Sotiropoulos M, Prezado Y. A scanning dynamic collimator for spot-scanning proton minibeam production. *Sci Rep.* 2021;11(1):18321. <https://doi.org/10.1038/s41598-021-97941-w>
  28. Sechopoulos I, Rogers DWO, Bazalova-Carter M, et al. RECORDS: improved reporting of Monte Carlo radiation transport studies: report of the AAPM Research Committee Task Group 268. *Med Phys.* 2018;45(1):e1-e5. <https://doi.org/10.1002/mp.12702>
  29. Faddegon B, Ramos-Méndez J, Schuemann J, et al. The TOPAS tool for particle simulation, a Monte Carlo simulation tool for physics, biology and clinical research. *Phys Med.* 2020;72:114-121. <https://doi.org/10.1016/j.ejmp.2020.03.019>
  30. Perl J, Shin J, Schumann J, Faddegon B, Paganetti H. TOPAS: an innovative proton Monte Carlo platform for research and clinical applications. *Med Phys.* 2012;39(11):6818-6837. <https://doi.org/10.1118/1.4758060>
  31. De Marzi L, Da Fonseca A, Moignier C, et al. Experimental characterisation of a proton kernel model for pencil beam scanning techniques. *Phys Med.* 2019;64:195-203. <https://doi.org/10.1016/j.ejmp.2019.07.013>
  32. Curtis HJ. The use of a deuteron microbeam for simulating the biological effects of heavy cosmic-ray particles. *Radiat Res Suppl.* 1967;7:250-257. <https://doi.org/10.2307/3583718>
  33. Hopewell JW, Trott KR. Volume effects in radiobiology as applied to radiotherapy. *Radiother Oncol J Eur Soc Ther Radiol Oncol.* 2000;56(3):283-288. [https://doi.org/10.1016/s0167-8140\(00\)00236-x](https://doi.org/10.1016/s0167-8140(00)00236-x)
  34. Rivera JN, Kierski TM, Kasoji SK, Abrantes AS, Dayton PA, Chang SX. Conventional dose rate spatially fractionated radiation therapy (SFRT) treatment response and its association with dosimetric parameters—a preclinical study in a Fischer 344 rat model. *PLoS ONE.* 2020;15(6):e0229053. <https://doi.org/10.1371/journal.pone.0229053>

**How to cite this article:** Ortiz R, De Marzi L, Prezado Y. Preclinical dosimetry in proton minibeam radiation therapy: robustness analysis and guidelines. *Med Phys.* 2022;49:5551–5561. <https://doi.org/10.1002/mp.15780>